7. Configuration Robustness and Flexibility

The QPS reference configuration was optimized for good neoclassical confinement and MHD stability and bootstrap alignment at $\langle\beta\rangle = 2\%$. The QPS modular coils, along with the value of the current in the outer VF coils and the auxiliary TF field, were then optimized to reconstruct the desired physics performance obtained for the original fixed-boundary configuration, subject to engineering constraints on the coils. The plasma obtained from a free-boundary VMEC reconstruction was found to have approximately the same physics properties (stability, transport, aspect ratio) as the fixed-boundary configuration for the same pressure and current profiles that were used in the original fixed-boundary configuration optimization.

However, to be useful for physics studies the QPS experiment must also:

(1) have good flux surfaces for the vacuum configuration (to promote ease of start-up);

(2) have a path from the initial (vacuum) state to the optimized (finite β or low ν^*) state (accessibility);

(3) be *robust* enough that it does not require only the optimized pressure and current profile for good performance (robustness against profile uncertainties and perturbations); and

(4) be *flexible* enough to explore a range of interesting magnetic configurations, not just the optimized magnetic configuration (flexibility).

7.1. Quality of the Vacuum Configuration

A requirement for a useful stellarator experiment is that it should have good flux surfaces in vacuum. This is necessary for both confirming that there are no significant field errors in the external coil configuration (as compared with the calculated vacuum configuration), and that low-β (low-power or low-ν^*) plasma configurations should be accessible for experimental study. Also, poor vacuum surfaces generally lead to poor plasma confinement and make it difficult to obtain the higher-parameter plasmas of interest.

Vacuum flux surfaces are calculated by following magnetic field lines with the AVAC Biot-Savart code.[1] Convergence studies show that accurate results for the flux surfaces and $\iota(r)$ are obtained when each coil is represented by 100 segments and field lines are followed for up to 100 toroidal transits. Figure 7.1 shows the last closed flux surface (LCFS) obtained for the free-boundary VMEC vacuum case and the flux surfaces obtained by following field lines. Both are calculated using the same representation for the coils and the same current in the modular, VF, and TF coil sets. While VMEC assumes good flux surfaces and cannot calculate magnetic islands or ergodic regions, AVAC makes no such assumption. For these coils, excellent agreement is obtained, and only a small region at the edge has broken surfaces. The case shown in the left side of Figure 7.1 is for the same current in the outer VF coils as for the $\langle\beta\rangle = 2\%$ reference case. The right side of Figure 7.1 shows that a reasonable fit is also obtained when the outer VF coil current is reduced by a factor 2 and the plasma is allowed to shift outward. In Figure 7.1, the flux surfaces from

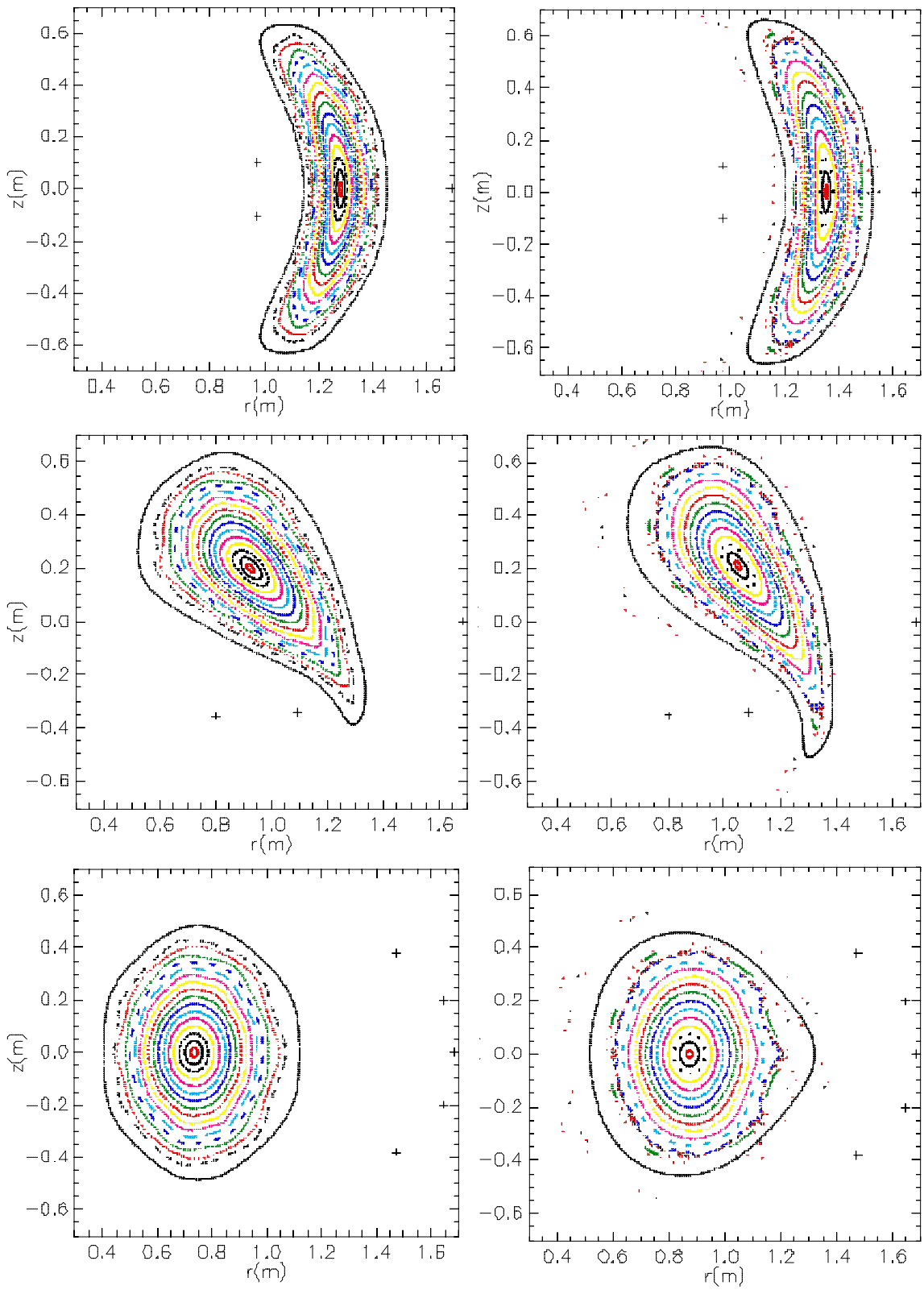

Figure 7.1. Flux surfaces from following field lines and the LCFS obtained from the free-boundary VMEC code for the vacuum case with I_{VF} = 204 kA (left) and 100 kA (right).

following field lines with AVAC are shown in color and the outer surfaces obtained from the free-boundary VMEC calculation are indicated by the outer black curve.

7.2. Accessibility of the Reference Configuration

Given good vacuum flux surfaces, another requirement is that the optimized finite-β magnetic configuration be accessible from the initial (vacuum) state. This capability has been examined by calculating a sequence of finite-β free-boundary equilibria in which the pressure profile shape was held fixed and the value of ⟨β⟩ was varied from 0 to 2% (Figure 7.2a). This modifies the rotational transform profile and shear as shown in Figure 7.2b. The main effect on the shape of the LCFS is a small outward shift (Figure 7.3), except at the half period location (Figure 7.3c) where the surface becomes more triangular as β increases. A similar effect can be obtained by changing the vertical field, as indicated in Figure 7.1.

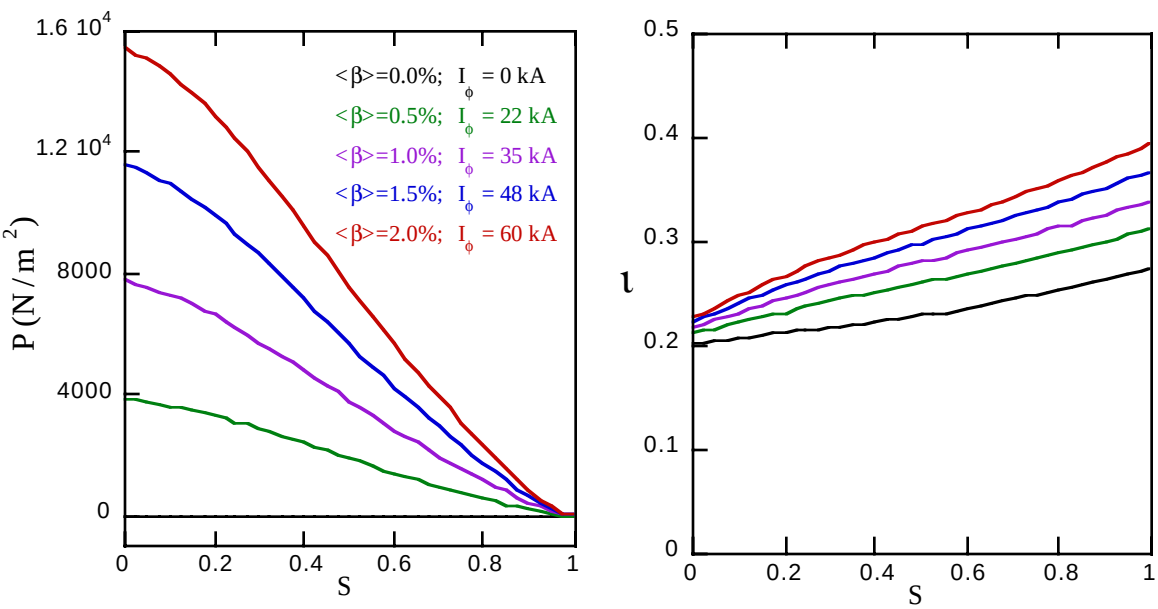

Figure 7.2. Varying the peak value of the pressure for a fixed profile shape (a) changes the shear in the rotational transform profile (b).

All the cases in the sequence are MHD stable to ballooning, kink, and vertical modes. The ballooning growth rate as calculated by the COBRA code is shown in Figure 7.4. The neoclassical confinement improves as ⟨β⟩ increases as indicated in Figure 7.5 by the decrease in the DKES L11 transport coefficients. Here L11 is the transport matrix coefficient relating particle (or energy) flux to the density (or temperature) gradient obtained from the DKES code. The corresponding value of the particle diffusivity D or the heat diffusivity χ is obtained by integrating the proper energy moment over the distribution function.

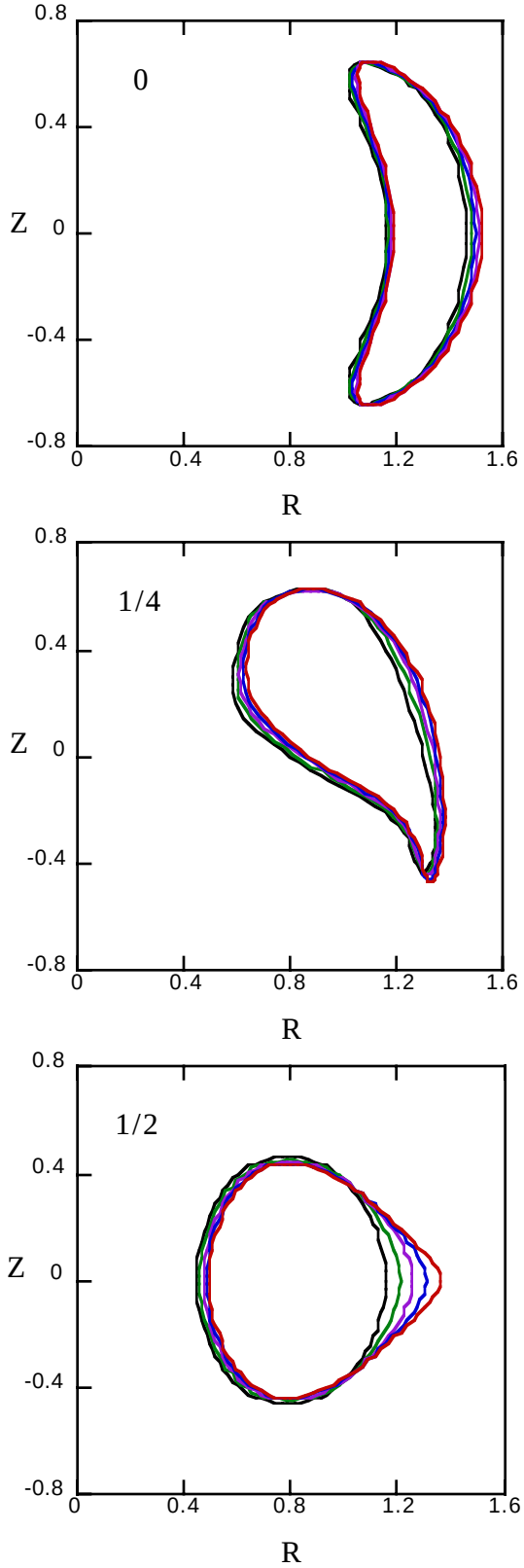

Figure 7.3. Outward shift of the LCFS in the β sequence.

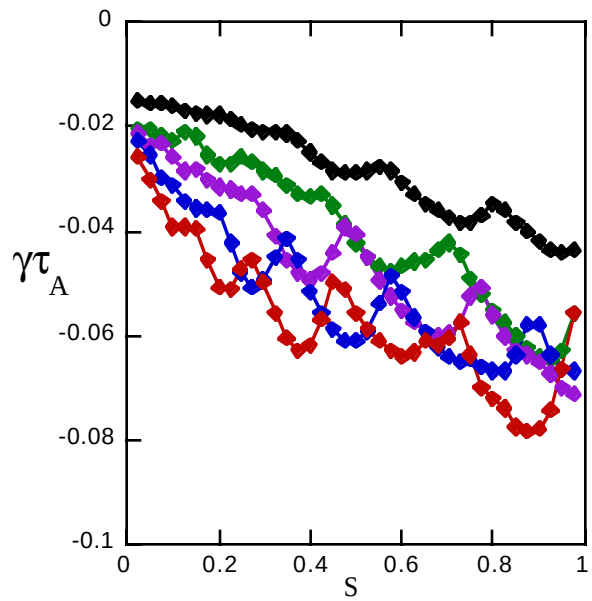

Figure 7.4. Ballooning growth rate normalized to the Alfven time as a function of the toroidal flux variable S ($\propto$ [r/a]^2) for the sequence shown in Figure 7.2.

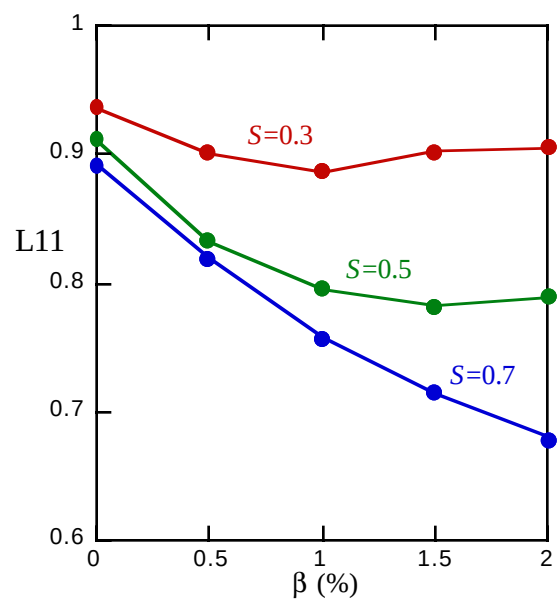

Figure 7.5. DKES L11 transport coefficients on the S = 0.3, 0.5, and 0.7 surfaces as a function of β for the sequence shown in Figure 7.2.

7.3. Robustness of the Reference Configuration

7.3.1. Profile sensitivity.

The pressure and surface-averaged parallel current profiles for the reference case plasma are shown in Figure 7.6. The reference current profile was chosen equal to the bootstrap current (this is so-called bootstrap "alignment" with the equilibrium current). To test the sensitivity of the reference

case to the pressure and current profiles, test profiles that are both more and less peaked than the reference case were chosen. These profiles are shown in Figure 7.7 and are consistent with the NCSX reference profiles [2].

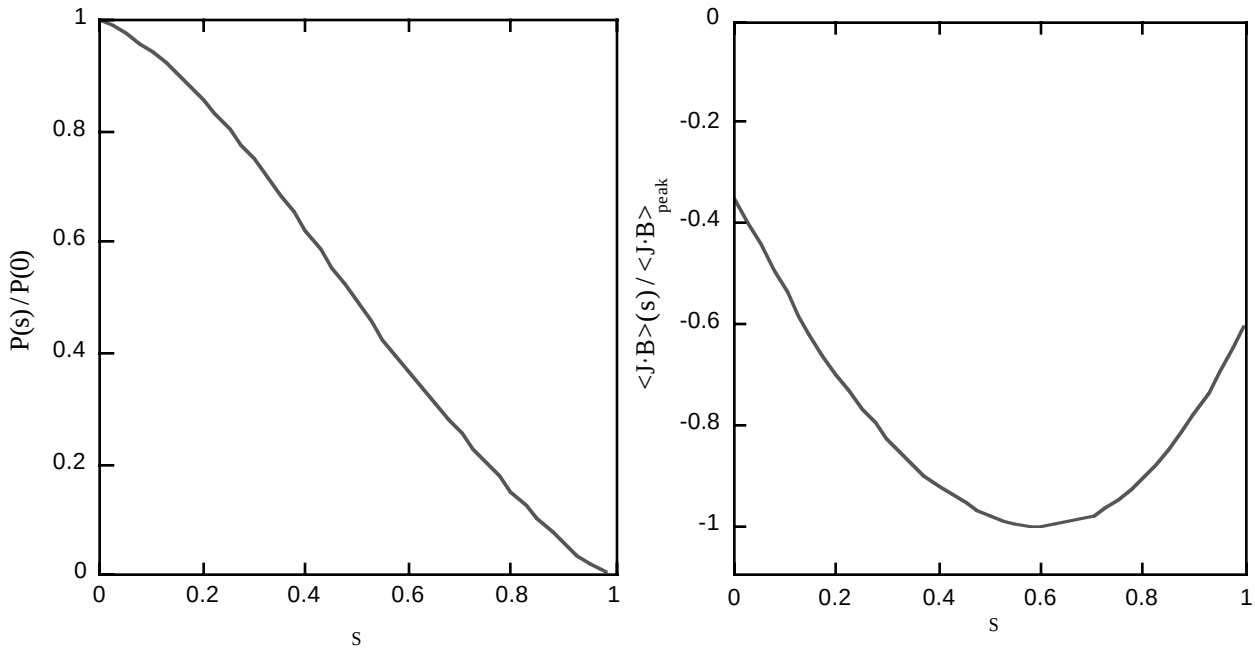

Figure 7.6. Reference pressure and surface-average parallel current profiles as a function of the normalized toroidal flux variable, S ~ $(r/a)^2$.

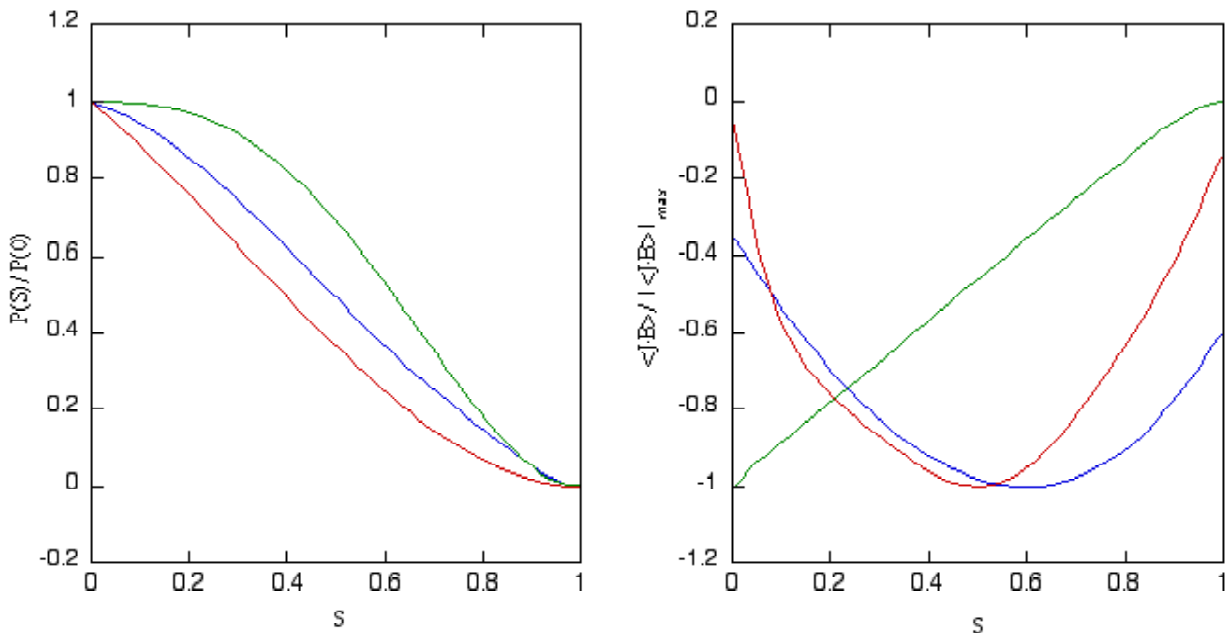

Figure 7.7. Test pressure and parallel current profiles. The reference profiles are shown in blue. For the pressure profiles, both a more peaked (red) and a flatter (green) profile were used. For the field-aligned current, an Ohmic profile (green) and a bootstrap profile with lower edge current (red) were used.

Effect of Profiles on Plasma Shape. All of these cases were run at $\langle\beta\rangle$ = 2% with a total toroidal current of 60 kA. The effect of the various current profiles on the plasma shape is shown in Figure 7.8. The cases shown in Figure 7.8 were all with the reference pressure profile. The effect of the different pressure profiles on the plasma shape is weaker than the effect of the various current profiles. While the plasma shape is sensitive to changes in $\langle\beta\rangle$ and the total toroidal current, it is only weakly affected by modifications in the pressure and current profiles.

Effect of Profiles on Rotational Transform. The rotational transform profile is, of course, more sensitive to modifications of the current profile and, to a lesser extent, changes in the pressure profile. Figure 7.9a shows the rotational transform profiles for the three different current profiles with the reference pressure profile. Using an Ohmic current profile, a weakly reversed shear profile is obtained. The two bootstrap current profiles (the reference case and the low-edge current case) have similar rotational transform profiles. Figure 7.9b shows the rotational transform profiles for the three different pressure profiles with the reference current profile. The variation of iota with the different test pressure profiles is similar for the other test current profiles. The pressure profile only has a large impact on the rotational transform if the current is forced to be bootstrap consistent (which was not the case for these calculations).

Effect of Profiles on MHD Stability. The effect of the test profiles on ballooning stability is shown in Table 7.1. The reference pressure profile is stable at $\langle\beta\rangle$ = 2% for the two bootstrap current profiles but the majority of surfaces are unstable for the Ohmic current profile. Indeed, for the Ohmic current profile all the cases were unstable on a majority of the surfaces (cases highlighted in red in Table 7.1). This is likely due to the very flat iota profile associated with the Ohmic current profile as shown in Figure 7.9a. Both the flatter and more peaked pressure profiles had regions of localized, weak ballooning instability for both the reference current profile. This is also the case for the more peaked pressure profile with the low-edge current bootstrap profile (cases highlighted in yellow in Table 7.1). This case can be made stable by lowering $\langle\beta\rangle$ to 1.9% (this was tested and confirmed for all the cases) or possibly by slightly modifying the pressure profiles (this was not tested). The flatter pressure profile with the low-edge current case was unstable over roughly a quarter of the surfaces with a maximum growth rate similar to the Ohmic cases. If the case is not stable on all surfaces, the numbers indicate the largest ballooning growth rate (normalized to the Alfvén time) and the fraction of surfaces unstable. Growth rates > 0.05 in these units are considered significant and difficult to stabilize with modest pressure profile variations. More details on the effect of Ohmic current on ballooning stability are described in the section 7.4.1.

Table 7.1. Effect of profiles on the ballooning stability.

<J·B>↓ P →	Reference	Flatter	More Peaked
Reference	Stable	0.052; 6/41	0.016; 3/41
Ohmic	0.098; 25/41	0.170; 22/41	0.127; 26/41
Low-edge bootstrap	Stable	0.099; 10/41	0.028; 6/41

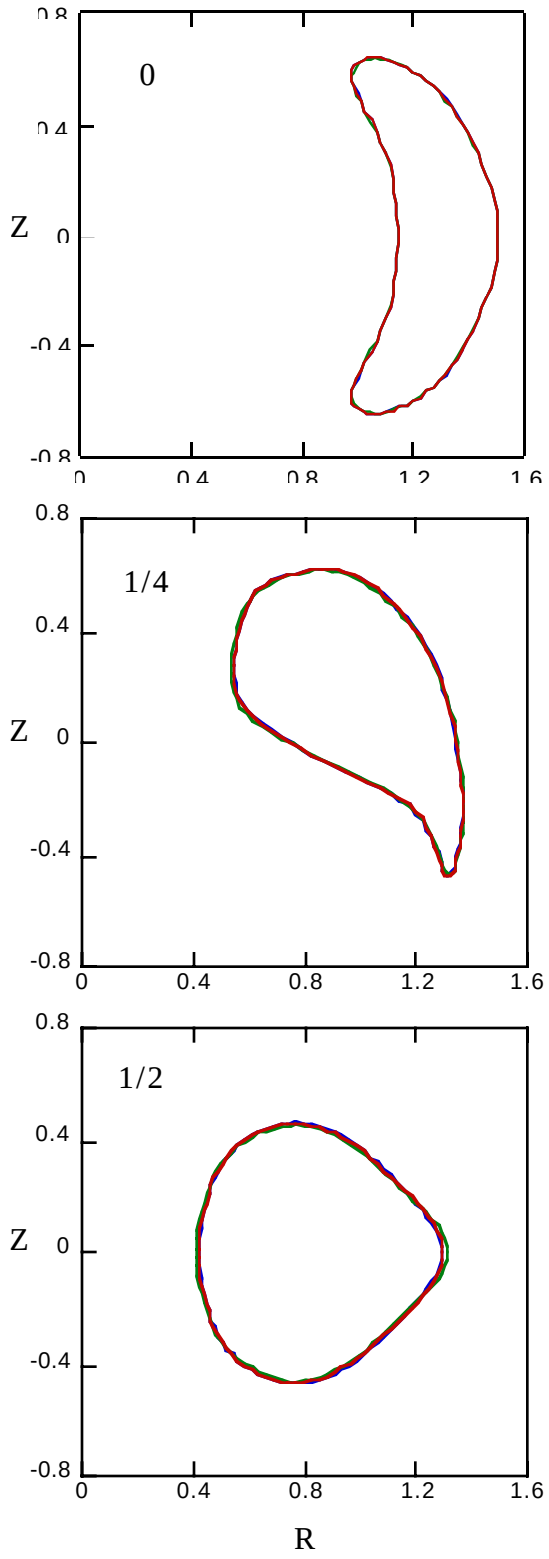

Figure 7.8. Cross sections of the outer flux surface at 0, 1/4, and 1/2 field periods. These cases are virtually indistinguishable, but, for reference, have colors that correspond to the different current profiles shown in Figure 7.5.

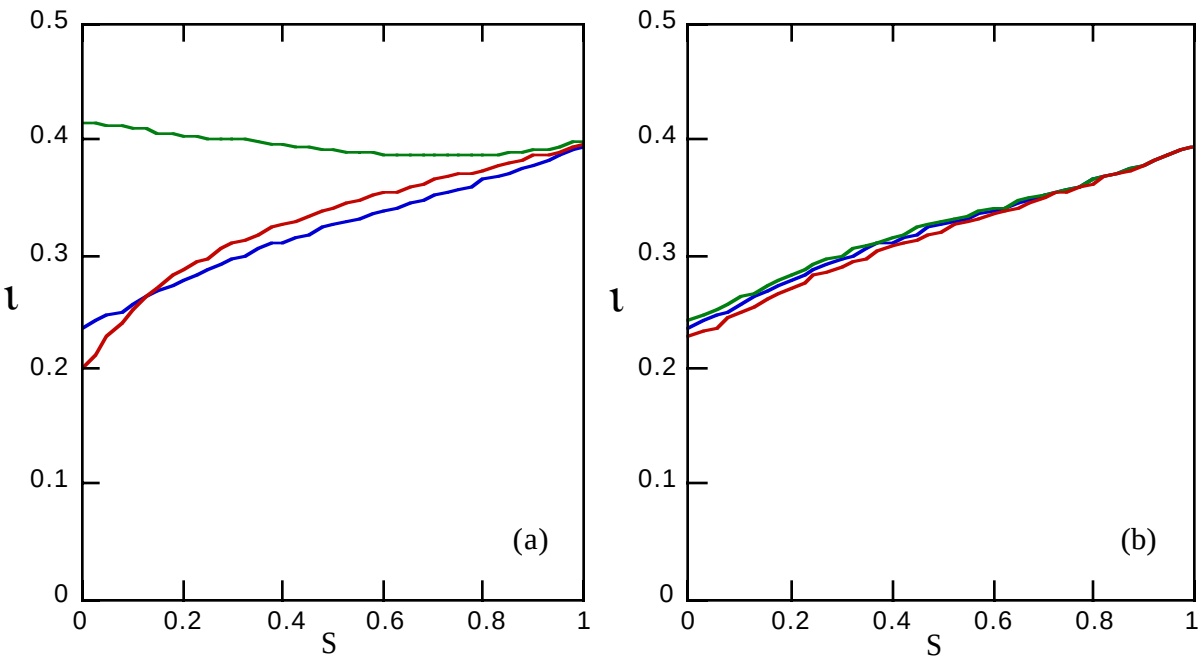

Figure 7.9. Rotational transform profiles for the (a) test current profiles with the reference pressure profile and (b) test pressure profiles with the reference current profile.

Effect of the Test Profiles on Confinement. The effect of the profile variation on transport was analyzed using the DKES transport code. The radial transport coefficient, L11, was calculated on three radial surfaces, $S = 0.3$, $S = 0.5$, and $S = 0.7$. The L11 transport coefficients for all the combinations of test pressure and current profiles are shown in Table 7.2. For all the pressure profiles, the Ohmic current profile had the lowest transport coefficients. This is likely a result primarily of the larger rotational transform associated with the Ohmic current profile. For the outermost surface tested ($S = 0.7$), the variation of L11 is ±6% around an average of 0.78. The pressure profile variation seems to have a weak effect on the transport coefficients (the exception being L11 on the $S = 0.3$ surface for the cases with an Ohmic current profile). We conclude that the transport is not sensitive to profiles.

Table 7.2. Effect of profiles on confinement as measured by the DKES transport code.

<J·B>↓ P →	Reference s = 0.3, 0.5, 0.7	Flatter s = 0.3, 0.5, 0.7	More Peaked s = 0.3, 0.5, 0.7
Reference	1.06; 0.91; 0.81	1.07; 0.93; 0.82	1.07; 0.90; 0.79
Ohmic	1.06; 0.77; 0.74	0.81; 0.79; 0.75	0.81; 0.75; 0.73
Low-edge bootstrap	1.02; 0.88; 0.78	1.03; 0.89; 0.79	1.03; 0.86; 0.77

7.4. Configuration Flexibility

The sets of modular coils, TF coils, VF coils, and the Ohmic current solenoid provide the flexibility needed to modify the plasma configuration to study modifications of equilibrium surface quality, MHD stability, and neoclassical transport. Different currents in the modular coils allow changing rotational transform and shear, the helical axis excursion, the mirror field component, the plasma shape, and the plasma aspect ratio. Currents in the VF coils can shift the magnetic axis radially and shape the plasma surface. Currents in the auxiliary TF coils ($\Delta B = \pm 0.15$ T) can change rotational transform and shear, and the OH solenoid (± 0.15 V-s) can be used to drive a plasma current and change or reverse the magnetic shear. The combination can be used to repair outer flux surfaces that were destroyed by magnetic islands, induce magnetic islands to bound the plasma or for open divertor studies, and test magnetic islands control and neoclassical tearing modes stability.

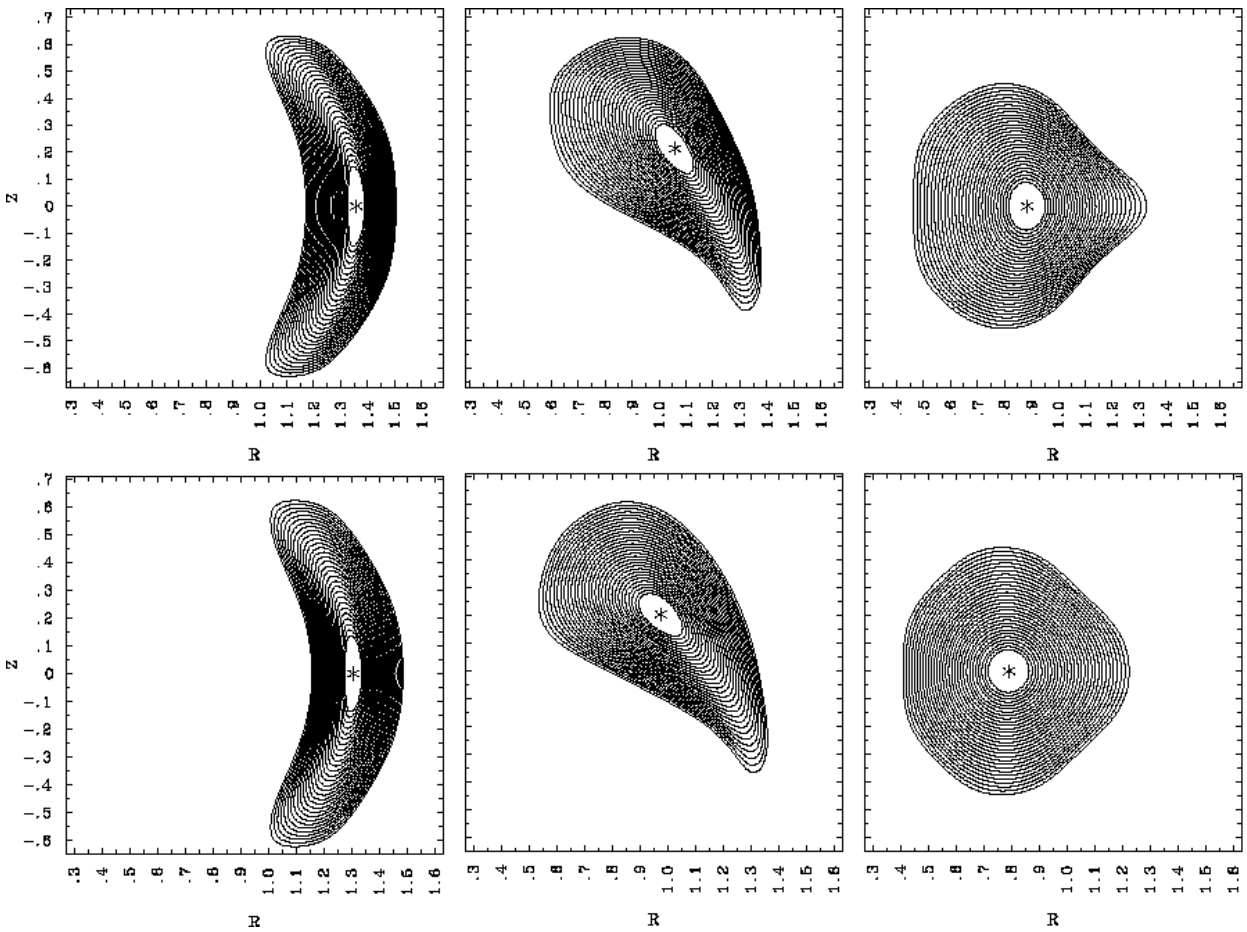

Figure 7.10. Cross sections of free-boundary flux surfaces at the beginning, 1/4, and 1/2 of a field period for a $\langle\beta\rangle = 2\%$ equilibrium with a 60-kA self-consistent bootstrap current profile (top row) and a 60-kA Ohmic current peaked on axis (bottom row).

7.4.1. Ohmic current.

The QPS experiment will have the capability to operate with both Ohmic-driven current and bootstrap-aligned current. This is confirmed in Figure 7.10 which shows the free-boundary flux surfaces for the $\langle\beta\rangle$ = 2%, $I_{bootstrap}$ = 60 kA case and a case with $\langle\beta\rangle$ = 0 and I_{Ohmic} = 60 kA. The finite-β bootstrap current and the Ohmic current produce have different current distributions and produce different rotational transform profiles (with opposite sign of the magnetic shear), as shown in Figure 7.11.

A sequence of $\langle\beta\rangle$ = 0 free-boundary VMEC calculations was done with the plasma Ohmic current varied through the similar values as in the $\langle\beta\rangle$ = 0 to 2% sequence in Figures 7.2 and 7.3. Figure 7.12 shows the assumed current density profiles and the resulting ι(r) as the Ohmic current is increased from 0 to 60 kA. The same improvement in neoclassical confinement with increasing current is seen in both cases (Ohmic vs. bootstrap current) despite the differences in the transform profile, as illustrated in Figure 7.13.

Figure 7.12 shows that the Ohmic current solenoid can be used to change the shear from stellarator shear (stabilizing) to tokamak shear (destabilizing) for studies of magnetic island control and stabilization of neoclassical tearing modes.

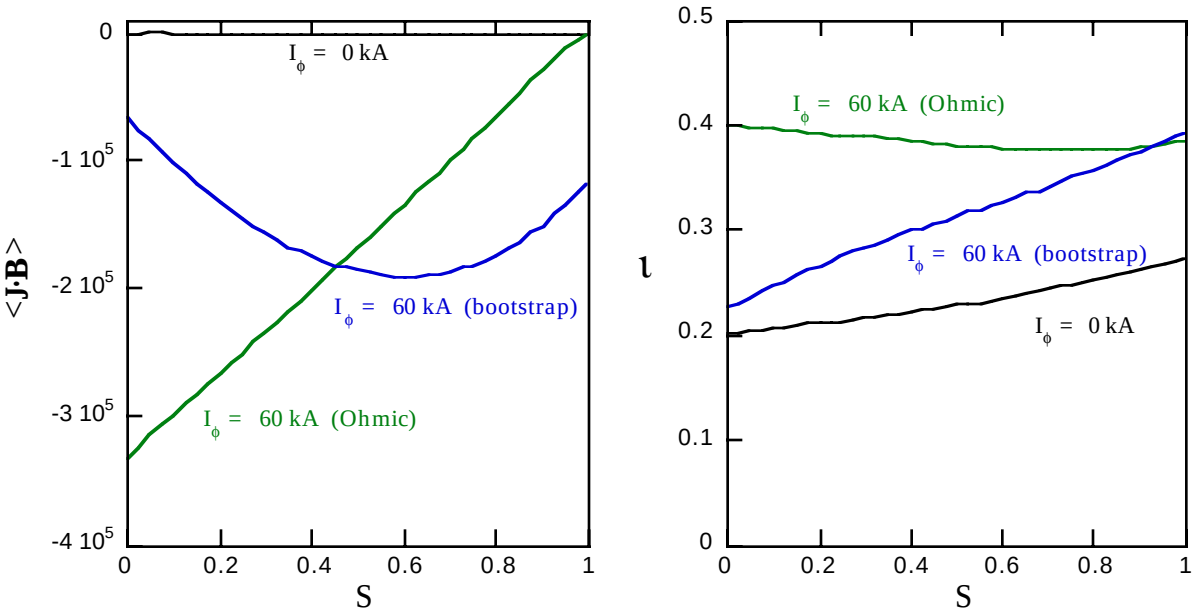

Figure 7.11. Free-boundary calculations of the rotational transform profile and current profile for Ohmic and bootstrap current for the QPS reference configuration.

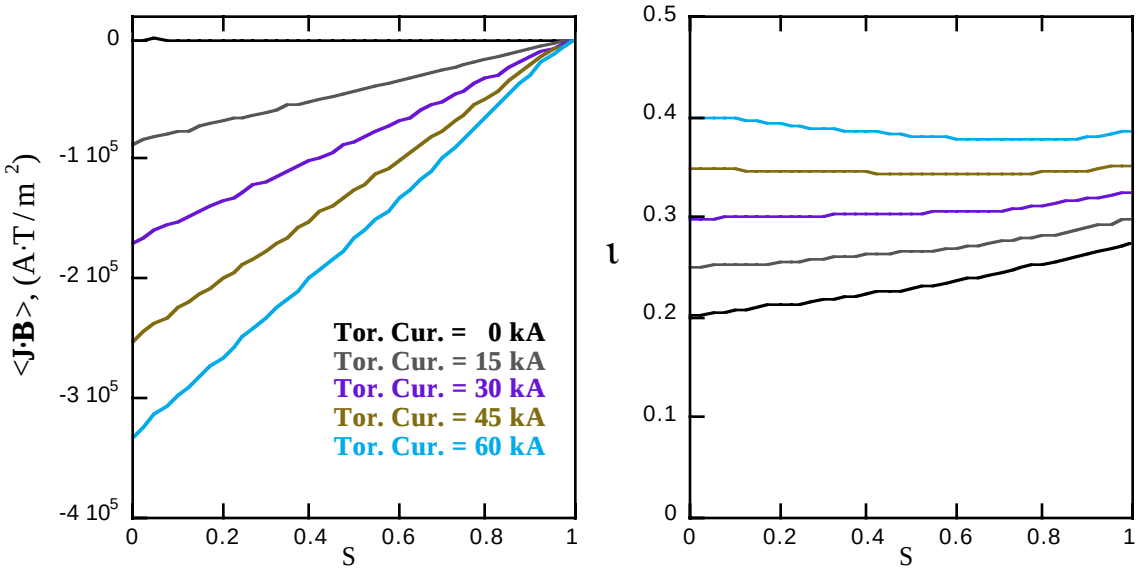

Figure 7.12. Ohmic profiles of field-aligned current and rotational transform as a function of the normalized toroidal flux.

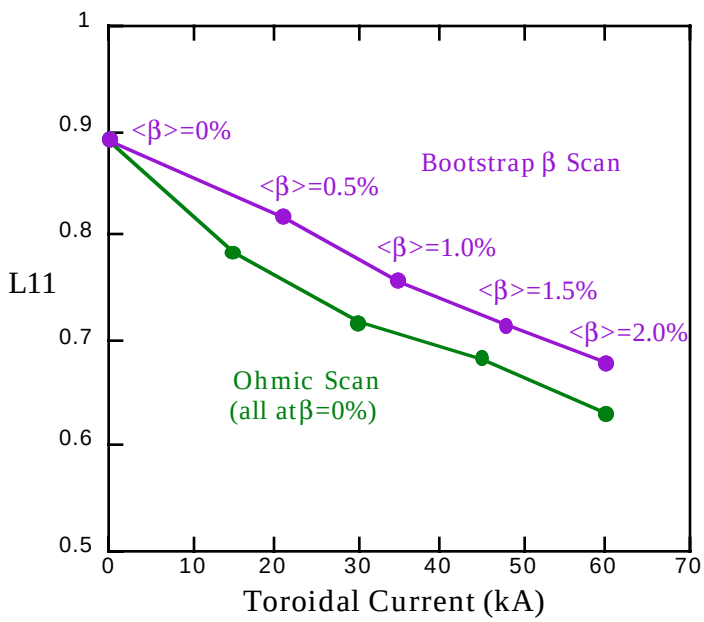

Figure 7.13. DKES L11 transport coefficient evaluated on the s = 0.7 surface as a function of the total toroidal current for an Ohmic current scan at $\langle\beta\rangle = 0$ and for the β scan shown in Figure 7.2.

7.4.2. Vertical Field control.

The vertical field coils can be used for controlling plasma positioning, shape, and rotational transform. The plasma equilibrium in the QPS device is sensitive to the current in the external vertical field coils. Vertical field scans have been conducted at both $\langle\beta\rangle = 0$ and $\langle\beta\rangle = 2\%$.

The rotational transform profiles at <β> = 0 for different values of the current in the vertical field coils are shown in Figure 7.14. As the current in the VF coils becomes more negative, the rotational transform profile increases in the core and decreases at the edge, reducing the shear across the profile. The field from the VF coils shifts the plasma to smaller major radius as the current in the VF coils becomes more negative. The minor radius is relatively unchanged as the VF coil current changes. The resulting variation of the aspect ratio is from 2.88 to 2.47 as I_{VF} goes from 0 to –200 kA, (-204 kA is the nominal design point for the reference configuration). The variation in *R* and *R*/*a* is shown in Figure 7.15.

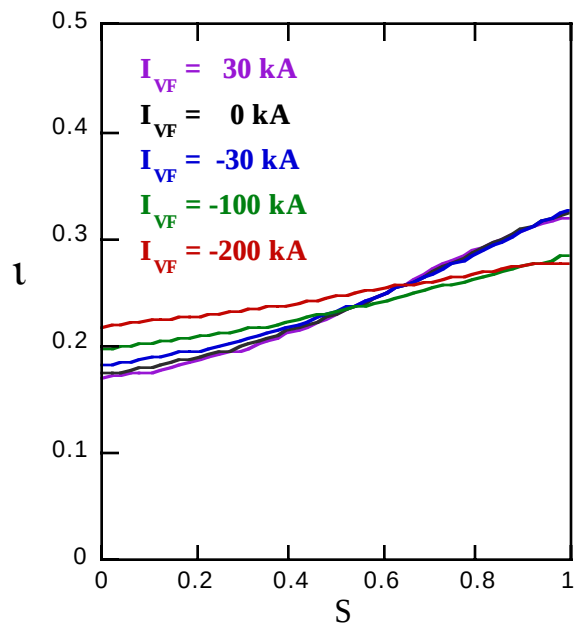

Figure 7.14. Rotational transform profiles as a function of the toroidal flux variable *S* for the reference configuration at β = 0 for different values of the current in the external vertical field coils.

At finite β (⟨β⟩ = 2%), the plasma equilibrium was more sensitive to variations in the vertical field. The VF coil current, I_{VF}, was varied from –185 to –216 kA (the value for the reference case is –205 kA). Within this range, the effect on the rotational transform profile was weak though the trend was the same as in the zero beta case: on axis, ι rises from 0.23 to 0.24, and at the edge, ι drops from 0.40 to 0.39 as I_{VF} goes from –185 to –216 kA. The plasma remained ballooning stable throughout this variation in I_{VF}. The DKES L11 coefficients had a 5% variation within this range of variation of I_{VF} (with L11 decreasing as I_{VF} became more negative). The effect of varying the current in the vertical field coils on the plasma shape is shown in Figure 7.16. The field from the VF coils shifts the plasma to smaller major radius as the current in the VF coils becomes more negative.

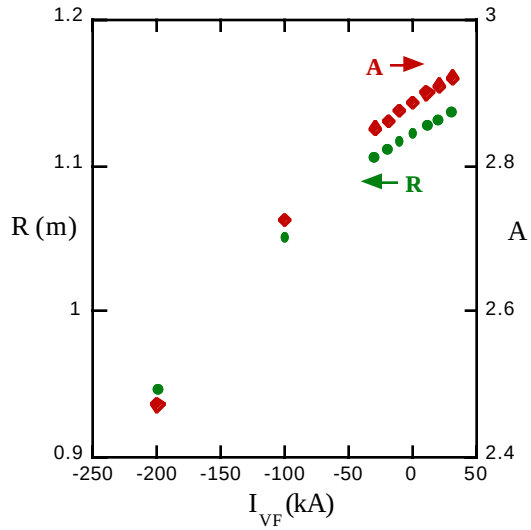

Figure 7.15. Variation of the major radius, R, and aspect ratio, *R*/a, at ⟨β⟩ = 0 as a function of the current in the vertical field coils.

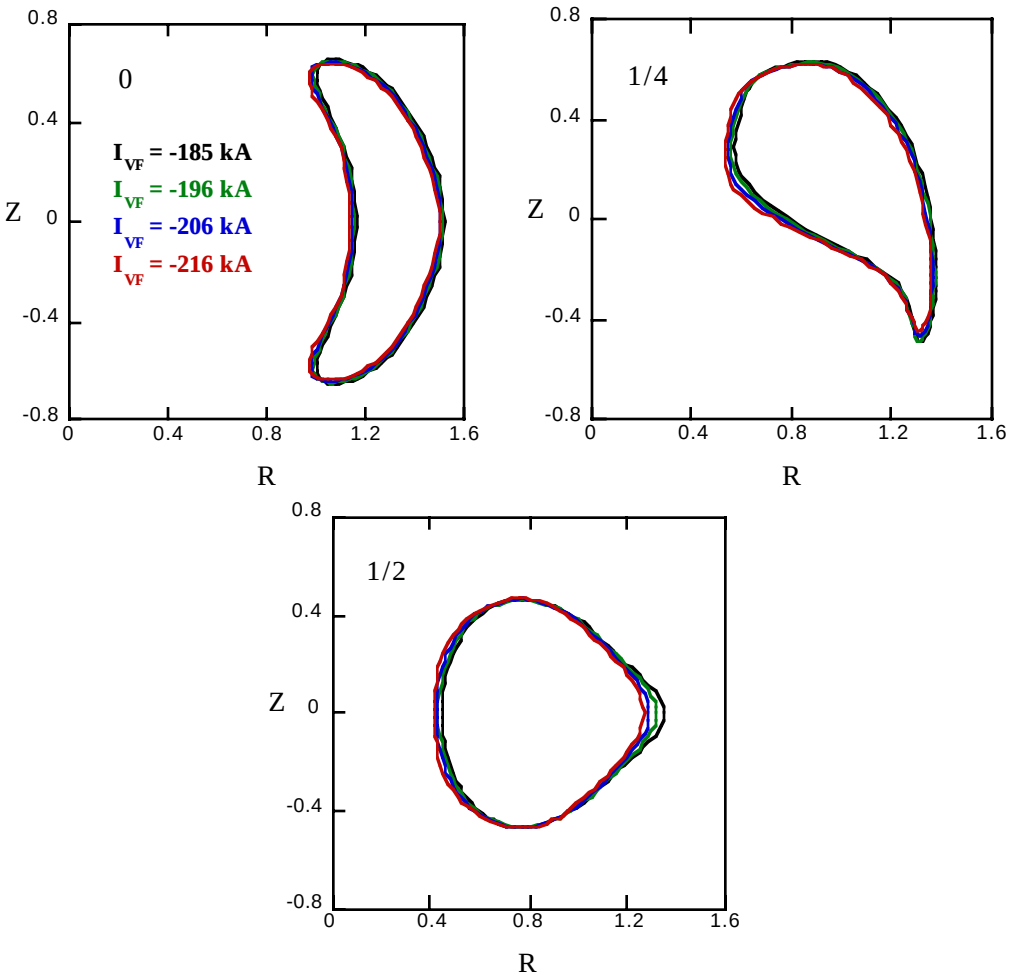

Figure 7.16. Cross sections of the outer surfaces of free-boundary equilibria at <β>=2% for the reference case for different values of the current in the vertical field coils.

7.4.3. Auxiliary TF Coils.

The QPS experiment will have the flexibility to vary the external toroidal field by roughly ±0.15 T, or ±15% at <|B|> = 1 T and ±30% at <|B|> = 0.5 T. To test the effect of varying external toroidal field on the plasma equilibrium, the current in the toroidal field coils was varied by ±20% and ±40% from the reference value of 259 kA. Overall this variation had little effect on the plasma equilibrium. The rotational transform profiles for this scan are shown in Figure 7.17. As the magnitude of the current in the external toroidal field coils is increased from 156 kA to 363 kA, the edge rotational transform increases from 0.38 to 0.41. This is due to the fact that the toroidal field generated by the external toroidal field coils subtracts from the toroidal field generated by the modular coils.

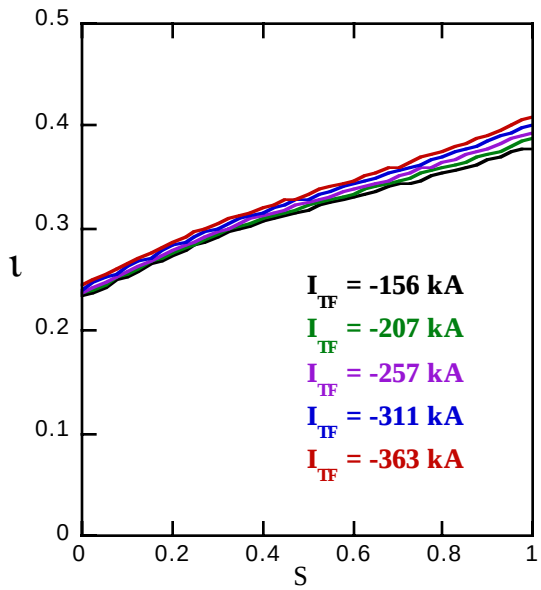

Figure 7.17. Rotational transform profiles for the reference case with the current in the external toroidal field coils varied by ±40% around the reference value of –257 kA.

The effect of the external toroidal field on the plasma shape is shown in Figure 7.18. As the current in the toroidal field coils becomes more negative, the plasma tends to become more elongated and in the 1/2 field period cross section it also becomes more triangular.

7.5. Summary.

Our studies indicate the following.

- Good vacuum magnetic surfaces exist for a range of mid-VF currents.
- The reference configuration with $\langle\beta\rangle = 2\%$ is accessible via a sequence of stable configurations with good transport at progressively higher β and self-consistent bootstrap current starting with $\beta = 0$ and no toroidal current.
- Pressure profile variations have a weaker effect on plasma shape than current profiles, but both have a weak effect.

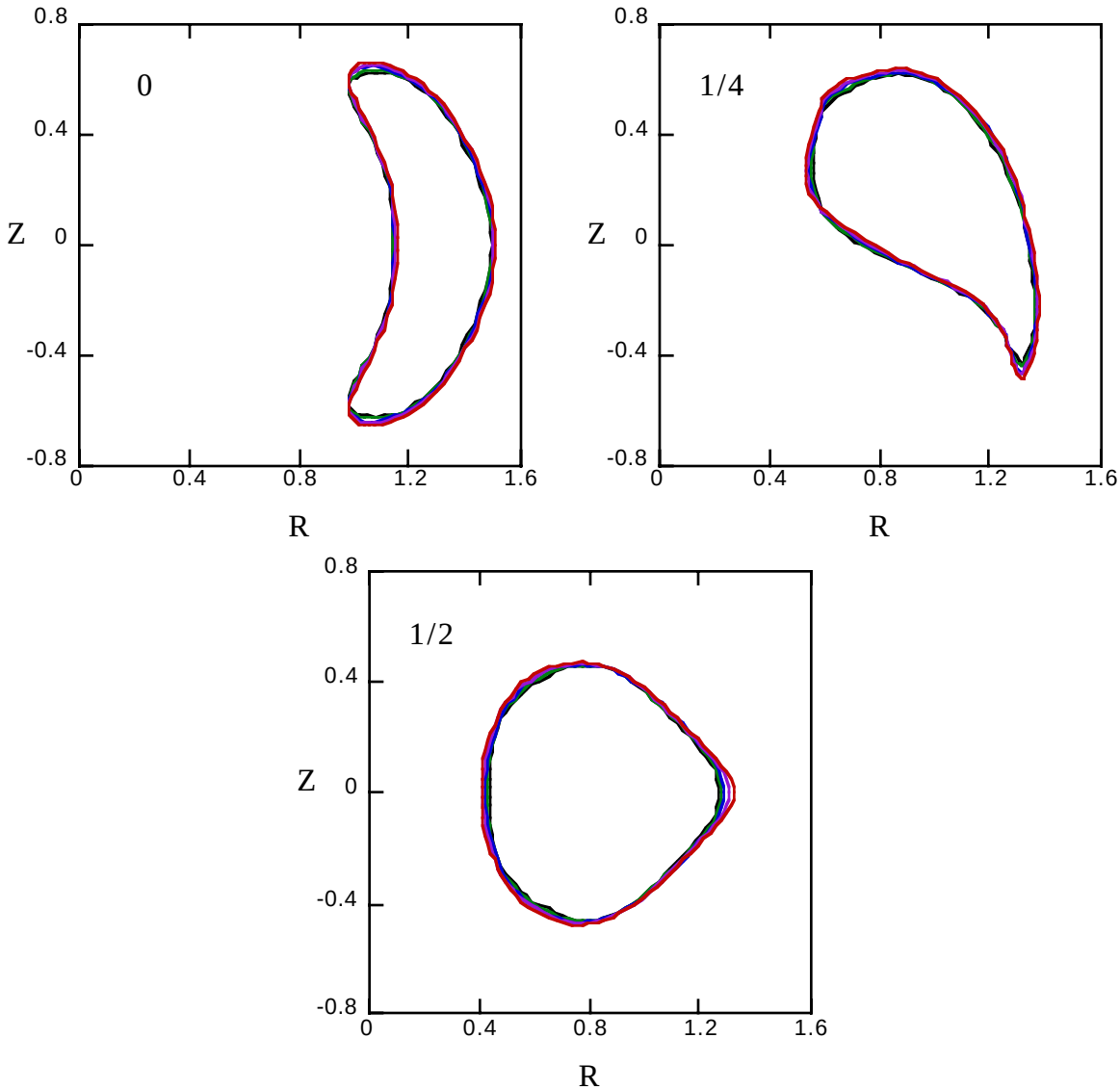

Figure 7.18. Variation in the outer surfaces as the cases shown in Figure 7.17.

- Ballooning stability is more sensitive to pressure profiles than current profiles. Both flatter and more peaked profiles lead to decreased stability. Ohmic-like current profiles are generally destabilizing.
- Transport is generally insensitive to profile variations.
- Ohmic current profiles reverse the sign of the shear from stellarator-like to tokamak-like shear.
- Transport improves with increasing current for both Ohmic currents at $\beta = 0$ and bootstrap current with self-consistent betas.
- Changing vertical fields results in a weak variation of the shear with modest variations in the plasma position, shape and confinement (for VF currents from –185 to –216 kA with a –204 kA reference level).

- The auxiliary TF field is mainly useful for tuning edge transform values for optimum surface quality.

References

[1] D. K. Lee, private communication.
[2] G. H. Neilson, A. H. Reiman, M. C. Zarnstorff, et. al., Physics of Plasmas **7**, 1911 (2000).